

EFFECT OF HORIZONTALLY INHOMOGENEOUS HEATING ON FLOW AND MAGNETIC FIELD IN THE CHROMOSPHERE OF THE SUN

P. SONG¹ AND V. M. VASYLIŪNAS^{1,2}

¹ Space Science Laboratory and Department of Physics, University of Massachusetts Lowell,
Lowell, MA 01854, USA; paul_song@uml.edu

² Max-Planck-Institut für Sonnensystemforschung, D-37077 Göttingen, Germany
Received 2014 August 19; accepted 2014 October 28; published 2014 November 12

ABSTRACT

The solar chromosphere is heated by damped Alfvén waves propagating upward from the photosphere at a rate that depends on magnetic field strength, producing enhanced heating at low altitudes in the extended weak-field regions (where the additional heating accounts for the radiative losses) between the boundaries of the chromospheric network as well as enhanced heating per particle at higher altitudes in strong magnetic field regions of the network. The resulting inhomogeneous radiation and temperature distribution produces bulk flows, which in turn affect the configuration of the magnetic field. The basic flow pattern is circulation on the spatial scale of a supergranule, with upward flow in the strong-field region; this is a mirror image in the upper chromosphere of photospheric/subphotospheric convection widely associated with the formation of the strong network field. There are significant differences between the neutral and the ionized components of the weakly ionized medium: neutral flow streamlines can form closed cells, whereas plasma is largely constrained to flow along the magnetic field. Stresses associated with this differential flow may explain why the canopy/funnel structures of the network magnetic field have a greater horizontal extent and are relatively more homogeneous at high altitudes than is expected from simple current-free models.

Key words: convection – magnetic fields – magnetohydrodynamics (MHD) – radiation mechanisms: thermal – Sun: chromosphere – waves

Online-only material: color figures

1. INTRODUCTION

The chromosphere and the corona remain poorly understood regions of solar-type atmospheres with many outstanding questions (see, e.g., Van de Hulst 1953; Parker 1965, 1991; Athay 1976; Withbroe & Noyes 1977; Böhm-Vitense 1984; Hollweg 1986; Narian & Ulmschneider 1990, 1996; Priest 2000; Ulmschneider 2001; Aschwanden 2005; Fossum & Carlsson 2005; Cranmer et al. 2007; Wedemeyer-Böhm et al. 2009). The rapid improvement of observational methods and techniques, particularly in recent years, has provided much new knowledge about chromospheric and coronal phenomena (see De Pontieu et al. 2007; Tsiropoula et al. 2012), but interpretations of these remote observations are often ambiguous and inconclusive.

In the search for an overall model to synthesize the observations, rather distinct problems are posed by the corona and by the chromosphere. The main puzzle of the corona is how to explain the very high temperatures, $1-2 \times 10^6$ K, with consequent full ionization of hydrogen. The required heating process must raise the temperature far above anything expected from simple thermodynamic considerations, but the amount of energy involved (not unambiguously determined) need not be large. In the chromosphere, the temperature profile is not understood in detail, but temperature values themselves are not extraordinary. The main problem is finding a heating process to supply energy that is radiated away (e.g., Withbroe & Noyes 1977; Vernazza et al. 1981), $\sim 3 \times 10^{29}$ erg s⁻¹, from the chromosphere (amounting to $\sim 10^{-4}$ solar luminosity from the photosphere). This represents $\sim 10^2$ the energy supply into the solar wind and ~ 10 the estimated coronal heating; in terms of total power, chromospheric heating is the largest dissipation process of the upper solar atmosphere.

Unlike both the corona above it and the solar interior below, the chromosphere for the most part is weakly ionized, and damping of Alfvén waves by collisional friction between plasma and neutrals has long been considered a possible mechanism for chromospheric heating (e.g., De Pontieu et al. 2001, 2007). Song & Vasyliūnas (2011) proposed, for chromospheric heating by strongly damped Alfvén fluctuations generated below the photosphere, a theoretical model from which wave damping, and hence the heating rate as function of altitude, could be calculated; they showed that both the rate and location of the energy input by this process are adequate to account for the observations. Subsequently, several studies and computer simulations have examined in detail the properties of Alfvén waves in the weakly ionized chromosphere and their consequences for heating and flow (e.g., Cheung & Cameron 2012; Khomenko & Collados 2012a, 2012b; Zaqarashvili et al. 2013; Soler et al. 2013a, 2013b; Shelyag et al. 2013), with an emphasis on local and small-scale aspects. In this Letter, we instead explore some global consequences of our model when horizontal spatial variations, in particular magnetic field structures associated with supergranulation, are taken into account; we find that these give rise to large spatial scale flows and field deformations, additional to and quite distinct from those of the Alfvén waves themselves. Because the heating process depends crucially on the presence of neutrals, our model does not apply directly to coronal heating.

In Section 2 we summarize the basic relations for determining temperature profiles; in Section 3 we review the essential properties of the heating process, emphasizing the dependence on the magnetic field, and in Section 4 the differing effects on plasma and neutrals; in Section 5 we describe the chromospheric flow produced by horizontally inhomogeneous heating and its

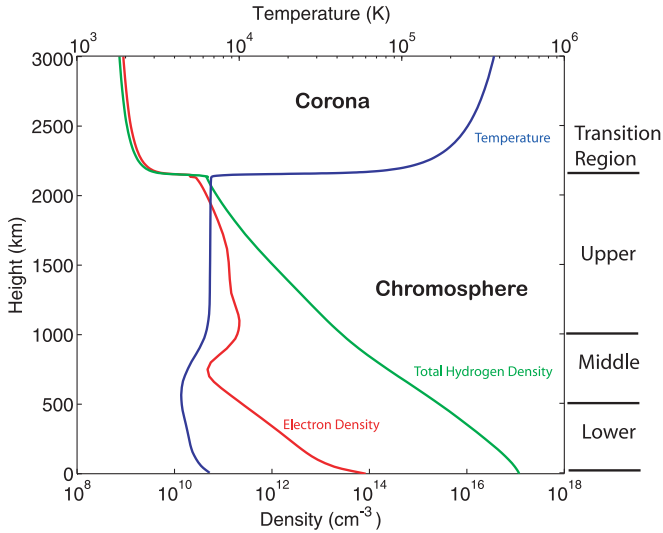


Figure 1. Temperature profile (blue), neutral hydrogen density (green), and plasma density (red) from a semi-empirical chromospheric model for the quiet Sun (Avrett & Loeser 2008).

(A color version of this figure is available in the online journal.)

interaction with the magnetic field; in Section 6 we summarize the essential physical points.

2. THERMAL EQUILIBRIUM OF THE QUIET CHROMOSPHERE

The empirical temperature profile shown in Figure 1 can be understood in terms of the thermal energy equation for the chromosphere:

$$(5/2)(d/dt)kT - kT(d/dt) \log P = (1/n)[\nabla \cdot \mathbf{q} + Q - R], \quad (1)$$

where $d/dt = \partial/\partial t + \mathbf{V} \cdot \nabla$ is the convective derivative, \mathbf{V} is the bulk velocity, n is the number density (concentration), T is the temperature, $P = nkT$ is the pressure, \mathbf{q} is the heat flux (usually assumed to be by conduction, $\mathbf{q} = -\xi \nabla T$ with ξ the heat conductivity coefficient), Q is the heating rate (Joule/ohmic heating plus collisional heating), and R is the radiative loss rate due to inelastic collisions; energy expended in collisional ionization may also be conveniently included in R . Equation (1) and subsequent equations refer to the medium as a whole, including both the neutral component (concentration n_n) and the plasma of electrons (n_e) and ions (n_i , connected to n_e by the charge quasi-neutrality condition); the relative amount of plasma is measured by the ionization fraction $x \equiv n_e/(n_e + n_n)$. Since collision rates are proportional to incident number density \times target density \times relative speed, one may write

$$R \simeq n^2 \Lambda(T, x), \quad (2)$$

where Λ is a function of temperature, composition, and ionization fraction, dependent on cross sections and rates for a variety of atomic-physics processes (e.g., Schmutzler & Tscharnuter 1993; Carlsson & Leenaarts 2012).

For large-scale thermal equilibrium of a quasi-static chromosphere, the left-hand side of Equation (1) may be neglected. The temperature profile is then determined by requiring that energy supplied by the heating process Q be removed by radiation loss R and heat conduction:

$$Q \simeq R - \nabla \cdot \xi \nabla T, \quad (3)$$

a differential equation which allows boundary conditions to be imposed at both the bottom and the top (which is important near the transition region). For a given temperature and ionization fraction, radiation loss varies as n^2 , while the heat-conduction term with classical heat conductivity (Spitzer 1956) is independent of n ; hence, radiation becomes relatively more important with decreasing altitude. Over much of the chromosphere, heat conduction can be neglected and the thermal equilibrium requirement reduced to the local equation $Q \simeq R$. Then, if Q is known, the temperature can be calculated from

$$Q \simeq R = n^2 \Lambda(T, x) = P^2 \Lambda(T, x) / (kT)^2, \quad (4)$$

with pressure constrained by the gravitational hydrostatic equilibrium. The resulting temperature profile (provided it is stable against convection and predicts a sufficiently small heat flux) is a valid first approximation for a quasi-static, horizontally stratified chromosphere.

3. PROPERTIES OF THE HEATING PROCESS

Song & Vasyliūnas (2011) showed that the heating rate from the damping of Alfvén waves propagating along the magnetic field from sources in or below the photosphere can be expressed as

$$Q(z, \omega) = F_0 \frac{B}{B_0} \frac{\omega^2}{V_{At}} \left[\frac{1-x}{v_{ni}} + \frac{v_e}{x \Omega_e \Omega_i} \right] \exp\left(-\frac{\omega^2}{\omega_1^2}\right) \quad (5)$$

with

$$\frac{1}{\omega_1^2} \equiv \int_0^z \frac{ds}{V_{At}} \left[\frac{1-x}{v_{ni}} + \frac{v_e}{x \Omega_e \Omega_i} \right]. \quad (6)$$

Here ω is the wave frequency, V_{At} is the Alfvén speed (with total mass density, plasma + neutrals), v_{ni} , v_e are the neutral-ion and electron collision frequencies and Ω_e , Ω_i the electron and ion gyrofrequencies, respectively, F is the wave energy flux density, and B is the magnetic field magnitude, where subscript $_0$ denotes the quantities at the source; the integral in Equation (6) is taken along the magnetic field line from source to altitude z . Integrating Equation (5) over frequency spectrum gives the total heating rate $Q(z)$; for an assumed power-law spectrum ω^{-k} above a minimum frequency ω_0 , Song & Vasyliūnas (2011) obtained an analytic expression for $Q(z)$ in terms of incomplete gamma functions. Tu & Song (2013) simulated the heating process by numerically solving collisional MHD equations in a one-dimensional chromosphere, without the local propagation and monochromatic wave approximations of the analytic model and with an allowance for wave reflection at the transition region as well as throughout the chromosphere; the simulation results agree with the predictions of the analytic model.

The main qualitative properties of the heating process can be inferred from Equations (5) and (6). Within the square brackets, the first term represents collisional heating from the plasma/neutral bulk flow difference, and the second represents ohmic heating. The collisional term, inversely proportional to ion density, is dominant at higher altitudes; the ohmic heating term, directly proportional to total density and inversely proportional to the square of the local magnetic field magnitude, is dominant at lower altitudes and for weaker fields. The coefficient in front of the square brackets in Equation (5) is independent of the local magnetic field. The exponential decrease with increasing frequency, above a cut-off ω_1 which decreases with increasing altitude, occurs because energy expended in heating

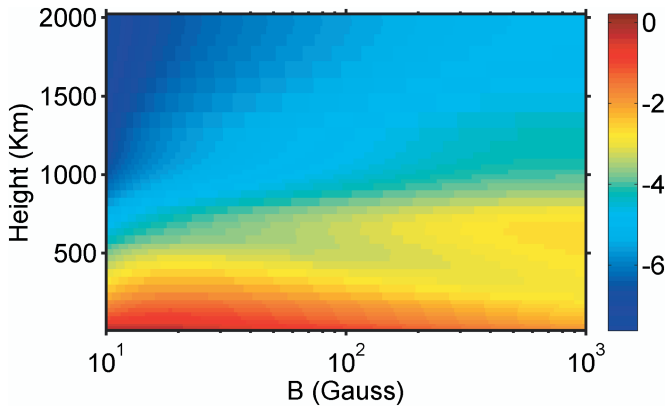


Figure 2. Logarithm of heating rate ($\text{erg cm}^{-3} \text{s}^{-1}$), with input $F_0 = 10^7 \text{ erg cm}^{-2} \text{s}^{-1}$, frequency-spectrum minimum $\omega_0/2\pi = 1/300 \text{ s}$, and power-law index $k = 5/3$.

(A color version of this figure is available in the online journal.)

is supplied by waves propagating from below, hence heating at any location reduces the energy available at higher altitudes; with heating rate proportional to ω^2 , high-frequency waves are damped preferentially. At a fixed altitude z , ω_1 increases with an increasing magnetic field averaged over altitude from z down to the source location, as defined by Equation (6).

The heating rate per unit volume Q in general decreases with increasing altitude and with increasing magnetic field. With increasing B , Q decreases at lower altitudes where ohmic heating (associated with electron collisions and proportional to $1/B^2$) dominates and increases at higher altitudes where frictional heating associated with ion-neutral collisions dominates (Vasyliūnas & Song 2005; Song & Vasyliūnas 2011); frictional heating itself is independent of B , but reduced damping at large B allows more wave energy to reach higher altitudes. The heating rate per particle Q/n , the quantity of primary interest for describing dynamical effects (e.g., on flow and magnetic field), increases with increasing altitude because of steeply decreasing density and increases at high altitudes with increasing magnetic field for the same reason as Q : a stronger field means less damping at low altitudes.

As an illustration, Figures 2 and 3 show the rates calculated from the analytic model of Song & Vasyliūnas (2011) as functions of altitude and local magnetic field (taken as constant; any assumed altitude variation can be accommodated by appropriate relative shifting). Figure 2 shows the heating rate Q . The distinction between low- and high-altitude regions is clearly apparent. With a magnetic field less than 20 G in most regions on the quiet Sun (Tsiropoula et al. 2012), the heating rate can reach values higher than the $10^{-1} \text{ erg cm}^{-3} \text{ s}^{-1}$ required to sustain radiative losses at lower altitudes (Withbroe & Noyes 1977). Figure 3 shows the heating rate per particle Q/n . The marked increase with increasing altitude is very apparent, particularly for strong fields. For weak fields, ohmic heating has removed so much energy at low altitudes that the heating rate (supplied by the remainder) decreases with altitude faster than the density until very high altitudes are reached; one result of this vertical variation is a pronounced minimum in Q/n , at an altitude $\sim 600 \text{ km}$ for $B \sim 10 \text{ G}$ and occurring lower with increasing B (a possible relation to the minimum in the temperature profile of Figure 1 is a subject of investigation).

The collisional heating mechanism described by Song & Vasyliūnas (2011) acts on both ionized and neutral components, imparting equal amounts of thermal energy to each. In a weakly ionized medium, this means much more energy per plasma

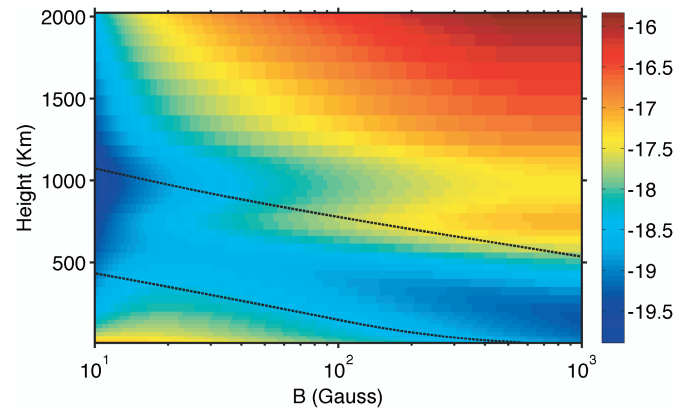


Figure 3. Logarithm of heating rate per neutral particle Q/N (erg s^{-1}), with constant input $F_0 = 10^7 \text{ erg cm}^{-2} \text{ s}^{-1}$ at a lower boundary. Dashed lines: $v_{\text{in}} = \Omega_i$ and $v_e = \Omega_e$.

(A color version of this figure is available in the online journal.)

particle; the implied excess of plasma over neutral temperature, however, is opposed by collisions that transfer energy from the hotter component to the cooler component (Vasyliūnas & Song 2005). With the collision rate in the chromosphere sufficiently high to keep the temperatures of ionized and neutral components nearly equal, the net heating rate is proportional to the relative fraction of each.

4. EFFECT OF HEATING ON FLOW OF IONIZED AND NEUTRAL COMPONENTS

Spatially inhomogeneous heating (Section 3), by creating and/or modifying temperature/pressure gradients, affects the bulk flow \mathbf{V} of the medium as a whole (plasma + neutrals), which is subject to pressure, gravity, and magnetic force (but no net collisional force):

$$\begin{aligned} (d/dt)\mathbf{V} = & -\nabla kT/m - (kT/m)\nabla \log(\rho + \rho_n) \\ & + \mathbf{J} \times \mathbf{B}/(\rho + \rho_n) + \mathbf{g}, \end{aligned} \quad (7)$$

where \mathbf{J} = current density, \mathbf{g} = gravity, and ρ , ρ_n are the plasma and neutral mass densities, respectively, and same for both has been assumed. The bulk flows of the two need to be treated separately, however, even when subject to the same heating per particle, because the ionized component is affected by the magnetic field but the neutral component (which is dominant in much of the chromosphere) is not. Plasma-neutral collisions act to eliminate any bulk-velocity difference, which therefore can exist only if collisional friction is opposed by other forces acting differently on plasma and neutrals. Subtracting the plasma and neutral-gas momentum equations gives

$$\begin{aligned} (d/dt)(\mathbf{V}_p - \mathbf{V}_n) + (v_{\text{in}} + v_{\text{ni}})(\mathbf{V}_p - \mathbf{V}_n) \\ = \mathbf{J} \times \mathbf{B}/\rho - (kT/m)\nabla \log(\rho/\rho_n), \end{aligned} \quad (8)$$

showing that $\mathbf{V}_p \neq \mathbf{V}_n$ can be created and maintained only by (1) magnetic force and/or (2) the difference between plasma and neutral pressure gradients (equivalent, by the assumption of common temperature, to gradient of ionization fraction). The resulting neutral flow relative to plasma is directed against the magnetic force and toward higher ionization, with magnitude equal to driving force per mass divided by collision frequency (at most $0.3 - 1 \text{ m s}^{-1}$ for a force as large as solar gravity).

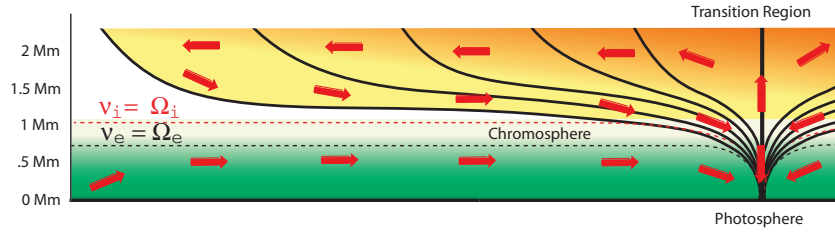


Figure 4. Two-dimensional illustration of a supergranule, qualitative but drawn approximately to scale with the correct ratio of the horizontal to vertical distance (symmetric right half of figure not shown). Solid lines: magnetic field lines. Red arrows: flow. Background color: regions of enhanced heating rate (green) or heating rate per particle (orange).

(A color version of this figure is available in the online journal.)

Additionally, plasma flow is subject to the generalized Ohm's law:

$$\mathbf{E} = -\mathbf{V}_p \times \mathbf{B} + (\mathbf{J} \times \mathbf{B}/n_e e) + \eta \mathbf{J} = -\mathbf{V}_e \times \mathbf{B} + \eta \mathbf{J}$$

$$\eta \equiv m_e v_e / n_e e^2, \quad (9)$$

which implies that for negligibly small resistivity η , the magnetic field is frozen to electron flow \mathbf{V}_e . With $\mathbf{J} = en_e(\mathbf{V}_i - \mathbf{V}_e)$, where \mathbf{V}_i is ion the bulk velocity, and $\mathbf{V}_i \simeq \mathbf{V}_p$ to the order of m_e/m_i , Equations (8) and (9) multiplied by $\times \mathbf{B}/B^2$ become

$$v_t(\mathbf{V}_p - \mathbf{V}_n) \simeq \Omega_i(\mathbf{V}_p - \mathbf{V}_e) \times \mathbf{B}/B + \dots$$

$$v_t \equiv v_{in} + v_{ni} \approx v_{in}$$

$$\Omega_e(\mathbf{V}_B - \mathbf{V}_{\perp e}) \simeq v_e(\mathbf{V}_p - \mathbf{V}_e) \times \mathbf{B}/B$$

$$\mathbf{V}_B \equiv \mathbf{E} \times \mathbf{B}/B^2, \quad (10)$$

showing how the various flows are related depending on collision-to-gyrofrequency ratios v_{in}/Ω_i , v_e/Ω_e .

5. CONSEQUENCES OF INHOMOGENEOUS HEATING

As an important example, we consider the configuration of the chromosphere associated with a supergranule: a quasi-two-dimensional structure of horizontal dimension about 30 Mm and vertical extent nominally about 2–2.5 Mm, with a highly inhomogeneous magnetic field as shown qualitatively in Figure 4, similar to the empirical composite of Wedemeyer-Böhm et al. (2009). At the bottom (interface to photosphere), a strong magnetic field (~ 1 kG) confined to a small region (~ 100 km) is surrounded by a weak field (< 10 G) elsewhere; at higher altitudes, as the (gravitationally stratified) confining gas pressure decreases exponentially, the field lines from the strong-field core (magnetic network) spread and ultimately cover much of the internetwork distance. The distribution of the magnetic flux across the bottom surface is determined by processes below the photosphere, as is the energy flux and spectrum of the Alfvén waves assumed to produce chromospheric heating. This configuration of the magnetic field, combined with field dependence of the heating rate (Section 3 and Figures 2 and 3), implies the inhomogeneous heating pattern illustrated by the shading in Figure 4: at high altitudes, heating per particle is largely confined horizontally to the central magnetic-network region but is greatly enhanced and increasing with altitude (reaching maximum approximately one scale height below full ionization, at which it goes to zero), while at low altitudes it is weaker and nearly uniform horizontally (except for depressed heating within the strong-field region). Note that the inhomogeneity of heating

results entirely from the magnetic network configuration; the wave energy source at the bottom surface has been assumed uniform, as the simplest first approximation.

If only pressure and gravity forces on the (dominant) neutral component are considered, the following flows are expected. Enhanced heating confined to a narrow region (here in the upper chromosphere) reduces, by expansion, the mass density of the medium and hence the downward gravitational force per unit volume, but (being localized) does not change the global upward pressure gradient. The resulting net upward force leads to upward flow within the narrow region of the strong magnetic field; in a quasi-steady state, the continuity of mass flow then imposes, as a consequence of the quasi-exponential density decrease (scale height ~ 150 km) required by gravitational stratification, a strong divergence of vertical flow and hence a global circulation pattern, with horizontal flow away from the strong-field region above and a return flow layer (thickness of the order of one scale height) below. Similarly, reduced heating confined to a narrow region (in the lower chromosphere) leads to downward flow and an associated circulation pattern (inflow toward the strong-field region) at lower altitudes; this flow is in the same direction as convection in and below the photosphere, associated with the supergranulation network (e.g., Parker 1978, 1979), and may be merged with it. The boundary between the two circulations is at an altitude where enhanced heating changes from horizontally localized to quasi-uniform.

The inclusion of plasma–neutral collisions and magnetic field constraints on plasma flow modifies the flow appreciably. The resulting flow pattern is illustrated in Figure 4, along with the critical altitudes where $v_e = \Omega_e$, $v_{in} = \Omega_i$. There are two principal effects.

1. The localized magnetic field of the network is too strong for plasma pressure of the weakly ionized chromosphere and is confined mainly by neutral-gas pressure. This implies that neutral-gas pressure must be higher outside the network than within it; furthermore, since neutral gas does not interact with the field except through collisions with plasma, there must be an inward flow of neutrals relative to plasma across the current layer bounding the strong-field region, described by Equation (8). The confined magnetic field reduces the buoyancy force by a factor $\beta/(1+\beta)$, where β = the ratio of the total (plasma + neutral) thermal to magnetic pressure.
2. Within the network, the altitude where $v_e = \Omega_e$ is at or below the photosphere, and $v_{in} = \Omega_i$ at $z \sim 500$ km. (Outside the network, $v_e = \Omega_e$ at $z \sim 500$ –700 km and $v_{in} = \Omega_i$ at $z \sim 1000$ km.)

Network magnetic field lines are thus effectively held attached to the photosphere, and plasma flow above $z \sim 500$ km,

except for mapped photospheric convection, is parallel to the magnetic field.

As a consequence, the upper circulation cells are, to first approximation, confined to the region threaded by the magnetic field lines from the network. The upward flow of the neutral component diverges horizontally to fill the expanding canopy–funnel-shaped region, with a downward return flow along the boundaries of the funnel. Plasma does not follow this neutral flow except along the magnetic field. The flow of neutrals but not of plasma across \mathbf{B} implies a current from Equation (8), which tends to widen the funnel. In other words, with a horizontal expansion that underlies the buoyancy force largely suppressed by the magnetic field and adverse external pressure, the effect of additional heating is mainly vertical expansion at a fixed altitude which increases the pressure above it. To balance the added pressure, the magnetic field expands further; the neutral flow implied by Equation (8) from the newly formed $\mathbf{J} \times \mathbf{B}$ constitutes the cross-field part of the circulation.

The lower circulation cells are not greatly modified.

6. DISCUSSION

Damped Alfvén waves propagating along the magnetic field from sources in or below the photosphere are likely present everywhere, but they produce very different heating within the supergranule magnetic network and outside it. In the internetwork weak-field region, most of wave energy is dissipated before the waves have propagated far, by the dominant ohmic heating (and possible altitude limit on field lines from the photosphere). Heating is thus enhanced at low altitudes, where its primary effect is to supply the energy radiated away (Song & Vasyliūnas 2011). Dynamical flow effects expected at the boundaries to the network are largely indistinguishable from the extended photospheric convection.

Within the strong-field network region, by contrast, ohmic heating and with it the entire damping is negligible at low altitudes; Alfvén waves can propagate to high altitudes along field lines that extend to the transition region and beyond, forming canopy-like structures covering much of the internetwork region. The dominant heating is by collisional plasma/neutral friction, and the heating rate per particle is high because of the low density. A significant temperature increase is thus produced within the spatially limited upper canopy–funnel-shaped part of the network (orange shaded region in Figure 4). Pressure readjustment to the changed temperature then leads to upward displacement and flow in the center, continuing as circulation of the neutral component outward to the sides and returning downward along the network boundaries; plasma is prevented from flowing across the field by MHD constraints. Although expected to be slow, this circulation can have appreciable consequences.

- Forces required to maintain the differential neutral–plasma flow tend to expand the canopy–funnel shape of the magnetic field lines even further sidewise. This may explain how network field lines emanating from isolated spots on the photosphere spaced some 20–30 Mm apart can create a nearly continuous canopy cover, with limited variability of field magnitude, at altitudes as low as 2 Mm. (Magnetic field models of this effect will be published elsewhere.)
- The formation of the localized strong surface fields of the network has been explained (Parker 1978, 1979) as the compression of a flux tube below the photosphere, by external pressure, when its interior temperature is lowered (relative to exterior) by the absence of nonadiabatic heating. The additional spreading of the canopy discussed above results from the same physics applied in reverse: expansion of the flux tube above the photosphere when its interior temperature is raised by the presence of nonadiabatic heating.
- Horizontal flow toward the strong-field core at mid-altitudes is shared by both photospheric/subphotospheric convection and chromospheric circulation. The former diverges downward as the network is approached. The latter contains a lower cell that also diverges downward (and is thus topologically part of the convection), plus an upper cell that diverges upward and then closes (neutral component only) by the horizontal flow away from the network. (The boundary between the two cells is interestingly close to the observed temperature minimum.)
- With the ionized component constrained to flow along field lines only, a plasma mass continuity problem arises whenever $\rho V_{\parallel}/B$ is not constant. Implications for ionization-fraction gradients (e.g., transition region) and time-varying effects possibly related, e.g., to type II spicules are subjects of investigation.

The authors thank E. H. Avrett and S. R. Cranmer for useful discussions and Y. Wang for preparing the figures. This study was supported by NSF grant AGS-0903777 and NASA grant NNX12AD22G to University of Massachusetts Lowell.

REFERENCES

- Aschwanden, M. 2005, *Physics of the Solar Corona: An Introduction with Problems and Solutions* (New York: Springer)
- Athay, R. G. 1976, *The Solar Chromosphere and Corona: Quiet Sun* (Astrophysics and Space Science Library, Vol. 53; Dordrecht: Reidel)
- Avrett, E. H., & Loeser, R. 2008, *ApJS*, 175, 229
- Böhm-Vitense, E. 1984, *Sci*, 223, 777
- Carlsson, M., & Leenaarts, J. 2012, *A&A*, 539, A39
- Cheung, M. C. M., & Cameron, R. H. 2012, *ApJ*, 750, 6
- Cranmer, S. R., van Ballegoijen, A. A., & Edgar, R. J. 2007, *ApJS*, 171, 520
- De Pontieu, B., Martens, P. C. H., & Hudson, H. S. 2001, *ApJ*, 558, 859
- De Pontieu, B., McIntosh, S. W., Carlsson, M., et al. 2007, *Sci*, 318, 1574
- Fossum, A., & Carlsson, M. 2005, *Natur*, 435, 919
- Hollweg, J. V. 1986, *JGR*, 91, 4111
- Khomenko, C., & Collados, M. 2012a, *ApJ*, 747, 87
- Khomenko, C., & Collados, M. 2012b, in *ASP Conf. Ser. 463, The Second ATST-EAST Meeting: Magnetic Fields from the Photosphere to the Corona*, ed. T. Rimmele et al. (San Francisco, CA: ASP), 281
- Narian, U., & Ulmschneider, P. 1990, *SSRv*, 54, 377
- Narian, U., & Ulmschneider, P. 1996, *SSRv*, 75, 453
- Parker, E. N. 1965, *SSRv*, 4, 666
- Parker, E. N. 1978, *ApJ*, 221, 268
- Parker, E. N. 1979, *ApJ*, 230, 905
- Parker, E. N. 1991, *ApJ*, 372, 719
- Priest, E. R. 2000, *Solar Magnetohydrodynamics* (Geophysics and Astrophysics Monographs; Dordrecht: Reidel)
- Schmutzler, T., & Tscharnuter, W. M. 1993, *A&A*, 273, 318
- Shelyag, S., Cally, P. S., Reid, A., & Mathioudakis, M. 2013, *ApJL*, 776, L4
- Soler, R., Carbonell, M., & Ballester, J. L. 2013a, *ApJS*, 209, 16
- Soler, R., Carbonell, M., & Ballester, J. L. 2013b, *ApJ*, 767, 171
- Song, P., & Vasyliūnas, V. M. 2011, *JGRA*, 116, A09104
- Spritzer, L., Jr 1956, *Physics of Fully Ionized Gases* (New York: Interscience)
- Tsiropoula, G., Tziotziou, K., Kontogiannis, I., et al. 2012, *SSRv*, 169, 181
- Tu, J.-N., & Song, P. 2013, *ApJ*, 777, 53
- Ulmschneider, P. 2001, *Encyclopedia of Astronomy and Astrophysics* (Bristol: Nature Publishing Group)
- Van de Hulst, H. C. 1953, in *The Sun*, ed. G. P. Kuiper (Chicago, IL: Univ. Chicago Press), 207
- Vasyliūnas, V. M., & Song, P. 2005, *JGRA*, 110, A02301
- Vernazza, J. E., Avrett, E. H., & Loeser, R. 1981, *ApJS*, 45, 635
- Wedemeyer-Böhm, S., Lagg, A., & Nordlund, Å. 2009, *SSRv*, 144, 317
- Withbroe, G. L., & Noyes, R. W. 1977, *ARA&A*, 15, 363
- Zaqarashvili, T. V., Khodachenko, M. L., & Soler, R. 2013, *A&A*, 549, A113